J Eng Math (2009) 64:303–315
DOI 10.1007/s10665-008-9259-6

EMHD free-convection boundary-layer flow from a Riga-plate

Asterios Pantokratoras · Eugen Magyari

Received: 28 May 2008 / Accepted: 13 November 2008 / Published online: 29 November 2008

Abstract The electro-magnetohydrodynamic (EMHD) free-convection flow of a weakly conducting fluid (e.g. seawater) from an electromagnetic actuator is considered. The actuator is a so called *Riga-plate* which consists of a spanwise aligned array of alternating electrodes and permanent magnets mounted on a plane surface. This array generates a surface-parallel Lorentz force which decreases exponentially in the direction normal to the (horizontal) plate. The free-convection boundary-layer flow induced by this body force is investigated numerically and analytically. It is shown that a certain length and velocity scale exists on which the flow characteristics are independent of the material properties of the fluid, as well as of the structural and functional parameters of the actuator. These *universal* velocity profiles are calculated numerically at different distances x from the leading edge and are discussed in some detail, both for the impermeable and the permeable Riga-plate when; in the latter case, a uniform lateral suction or injection of the fluid is applied. For the flow characteristics analytical approximations are reported. The asymptotic suction profiles approached for large values of x are given in exact analytical form. From a mathematical point of view the basic equations of the present boundary-value problem resemble those of the classical Blasius problem with an inhomogeneous forcing instead of an external flow and, accordingly, a homogeneous asymptotic condition.

Keywords Boundary layer · Electro-magnetohydrodynamic · Riga-plate

1 Introduction

Boundary-layer control is as old as the boundary-layer theory itself. Suction as an efficient means to control flow separation was described by Prandtl already in his pioneering paper of 1904. The physical reason of flow separation is a momentum deficit in the boundary layer which occurs when the fluid, decelerated by viscosity, runs into an adverse pressure gradient which cannot be overcome by its kinetic energy.

The flow of electrically conducting fluids can be controlled (in addition to the classical methods of suction, blowing and wall motion) with the aid of electromagnetic body forces which are able to compensate the mentioned

A. Pantokratoras (✉)
School of Engineering, Democritus University of Thrace, 67100 Xanthi, Greece
e-mail: apantokr@civil.duth.gr

E. Magyari
Institute of Building Technologies, ETH Zürich, 8093 Zürich, Switzerland

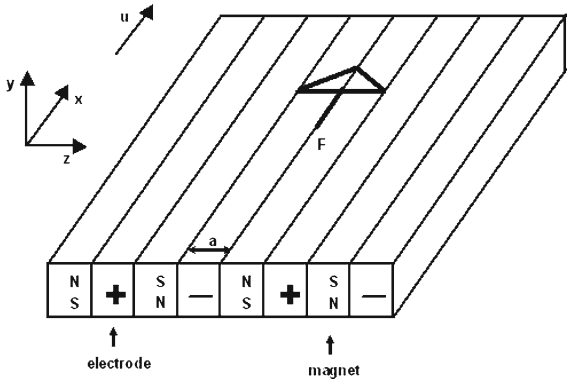

Fig. 1 Sketch of a Riga plate consisting of an alternating array of electrodes and permanent magnets. The Lorentz force and the mainstream velocity are parallel to the array

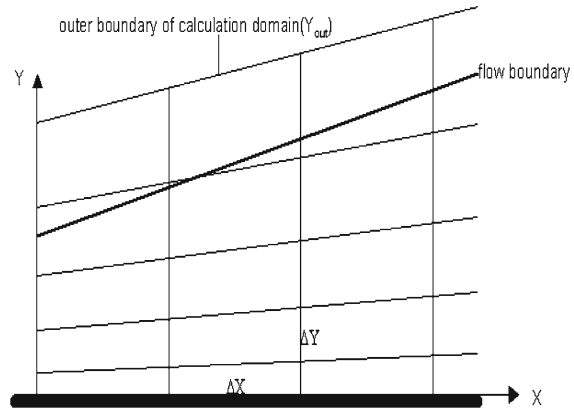

Fig. 2 The flow configuration and coordinate system

momentum deficit, by "energizing" the boundary layer. The motion of fluids of high electrical conductivity σ (e.g. liquid metals, semiconductor melts of $\sigma \sim 10^6$ S/m) can already be influenced significantly by external magnetic fields of moderate strengths of $\sim$1 T. This is the classical MHD flow control. In weakly conducting fluids (e.g. seawater of $\sigma \sim 10$ S/m), however, the currents induced by an external magnetic field alone are too small, and an external electric field must be applied to achieve an efficient flow control (EMHD flow control). A cross-wise electric and magnetic field e.g. can produce in this case a wall-parallel Lorentz force able to change the structure of a pressure-gradient-driven boundary layer and stabilize its motion by slowing down its growth.

An ingenious way to generate a wall-parallel Lorentz force was proposed in the sixties by Gailitis and Lielausis of the Physics Institute in Riga, Latvia [1]. The flow-control device of Gailitis and Lielausis is an electromagnetic actuator which consists of a spanwise aligned array of alternating electrodes and permanent magnets, mounted on a plane surface as sketched in Fig. 1. This set-up, sometimes referred to as *Riga-plate* [2] can be applied to reduce the friction and pressure drag of submarines by preventing boundary-layer separation as well as by diminishing turbulence production. As was proved few years later by Tsinober and Shtern [3] as an effect of the wall-parallel Lorentz force, the stability of the Blasius flow over the Riga plate is actually enhanced. In the boundary-layer calculations of Tsinober and Shtern [3] for the Lorentz force an averaged expression over the spanwise coordinate reported earlier by Grinberg [4] has been used. The most important feature of this *Grinberg-term* of the boundary-layer momentum equation is that it is fully decoupled from the flow. More precisely, the Gringerg term (i) is independent of the streamwise velocity u and (ii) it decreases exponentially with the coordinate y measured normal to the plate (see Eq. 1 below). These properties are in sharp contrast to those of the classical *Hartmann-term* $-\sigma B_0^2 u$ due to a uniform magnetic field B_0 applied in the y-direction, which acts on the forced-convection flow as a *magnetic brake*.

After two decades of stagnation, the research interest in Gailitis–Lielausis-type actuators was markedly renewed in the nineties, mainly with the aim of reducing the skin friction of turbulent boundary layers [5–9]. The effect of an oscillating wall-parallel Lorentz force in the spanwise direction has been investigated by numerical simulations by Kim [10] and Berger et al. [11]. In both papers substantial reductions of the skin friction in turbulent boundary layers were found. These predictions have been confirmed by the experiments of Pang and Choi [12]. Direct numerical simulations performed recently by Mutschke et al. [13] have once more confirmed the efficiency of oscillatory forcing in the separation flow control. Extensions of the electromagnetic control to flows over circular cylinders have been reported by Kim and Lee [14] and by Posdziech and Grundmann [15], and extensions to channel flows by Breuer et al. [16]. Comprehensive numerical simulations of drag reduction in a turbulent channel flow were presented recently by Shatrov and Gerbeth [17]. The first experimental results on the separation control of flow over hydrofoils were published only few years ago by Weier et al. [18] and Weier and Gerbeth [19]. The

electromagnetic drag reduction and wall-turbulence suppression by use of transverse traveling waves was examined by Du and Karniadakis [20] and by Du et al. [21]. The stability of the transitional boundary-layer flow subject to a wall-parallel Lorentz force has been investigated recently by Albrecht et al. [22], and a significant damping of the Tollmien–Schlichting waves already by moderate amplitudes of the applied force was reported. A systematic and comprehensive literature review of the development sketched above of electromagnetic flow control can be found in the PhD thesis of Weier [23]. The early stage of this development, as well as the contributions of the Dresden–Rossendorf Magnetohydrodynamics Group, are described by Weier [23] in great detail.

The aim of the present paper is to examine a very basic aspect of the boundary-layer flow of low electrical conductivity fluids over the Riga-plate. Namely, whereas the whole pertinent research effort has been focused so far on the control of flows driven by an external free stream, the aim of the present paper is to examine the *free-convection flow* induced by this electromagnetic actuator itself. More precisely, we assume that the only driving force of the boundary-layer flow over a horizontal Riga-plate is the electromagnetic body force described by the exponentially decaying *Grinberg-term* of the momentum equation. The characteristics of this free-convection *Gailitis–Lielausis–Grinberg flow* (hereafter *GLG flow*) are examined in the paper numerically and analytically in some detail.

2 Basic equations and nondimensionalization

We consider the electro-magnetohydrodynamic free-convection plane boundary-layer flow induced in a weakly conducting fluid by a so called *Riga-plate* [1–4]. The Riga-plate consists of an alternating array of electrodes and permanent magnets mounted on a plane surface as sketched in Fig. 1. The flow is driven over the horizontal plate solely by a Lorentz force directed parallel to the array. In addition to this electromagnetic body force, no other driving forces (pressure gradient, moving wall, etc.) are present.

In the general case, the volume density of the Lorentz force is given by the vector product $\mathbf{F} = \mathbf{j} \times \mathbf{B}$, where $\mathbf{j}$ is the electric current density induced in the fluid and $\mathbf{B}$ the magnetic induction. According to Ohm's law, the current density is obtained as $\mathbf{j} = \sigma\,(\mathbf{E} + \mathbf{v} \times \mathbf{B})$, where $\mathbf{E}$ denotes the electric field, $\mathbf{v}$ the fluid velocity and σ the electrical conductivity of the fluid. In the case of fluids of high electrical conductivity, $\sigma \sim 10^6$ S/m, a fully contactless flow control can be achieved without any external electric filed, since in this case already the current density $\sigma\,(\mathbf{v} \times \mathbf{B})$ induced by moderate applied magnetic fields of ~ 1 T is sufficiently strong (MHD flow control). In this case $\mathbf{F} = \mathbf{j} \times \mathbf{B} = \sigma\,(\mathbf{v} \times \mathbf{B}) \times \mathbf{B} = \sigma\left[(\mathbf{v} \cdot \mathbf{B})\,\mathbf{B} - B^2\mathbf{v}\right]$. However, in weakly conducting fluids of $\sigma \sim 10$ S/m or smaller, the current density $\sigma\,(\mathbf{v} \times \mathbf{B})$ is too small, even for magnetic fields of several Tesla. Accordingly, on low-σ fluids an external electric field must be applied to achieve an efficient flow control (EMHD flow control). In this case $\mathbf{F} = \mathbf{j} \times \mathbf{B} \approx \sigma\,(\mathbf{E} \times \mathbf{B})$, which implies that *in low-σ fluids the Lorentz force becomes independent of the flow field*.

In the case of the Riga-plate shown in Fig. 1, neglecting the edge-effects, both the applied electric and magnetic fields possess components only in the wall-normal direction y and the spanwise direction z. As a consequence, the resulting Lorentz force $\mathbf{F} = \sigma\,(\mathbf{E} \times \mathbf{B})$ points in the x-direction. Due to the stripwise structure of the plate, near to its surface strong spanwise variations of $\mathbf{F}$ occur [18], which, however, decrease rapidly with increasing distance y. As was first shown by Grinberg [4], the force density $\mathbf{F} = F\mathbf{e_x}$ averaged over the spanwise coordinate z becomes an exponentially decreasing function of y, namely

$$\langle F \rangle = \frac{\pi}{8}\, j_0 M_0 \exp\left(-\frac{\pi}{a}\, y\right), \tag{1}$$

where j_0 (A/m^2) is the applied current density in the electrodes, M_0 (Tesla) is the magnetization of the permanent magnets and a is the width of magnets and electrodes (see also [2], as well as the Appendix of [11]). Accordingly, the governing continuity and momentum-balance equations of the incompressible Gailitis–Lielausis–Grinberg (GLG) boundary-layer flow are

$$\frac{\partial u}{\partial x} + \frac{\partial v}{\partial y} = 0, \tag{2}$$

$$u\frac{\partial u}{\partial x}+v\frac{\partial u}{\partial y}=\upsilon\frac{\partial^2 u}{\partial y^2}+\frac{\langle F\rangle}{\rho}. \tag{3}$$

In the above equations u and v denote the velocity components in the x- and y-direction, respectively, υ is the kinematic viscosity and ρ the density of the fluid. As already mentioned, in contrast to the classical *Hartmann-term*, $-\sigma B_0^2 u/\rho$, the *Grinberg term*, $\langle F\rangle/\rho$, of the momentum equation does not depend on the flow velocity.

In the following considerations we generally assume that the plate is permeable and that a constant lateral suction or injection of the fluid may be applied. Accordingly, the boundary conditions are

$$u|_{y=0}=0,\quad v|_{y=0}=-v_0,\quad u|_{y\to\infty}\to 0. \tag{4}$$

Introducing the dimensionless quantities

$$X=\frac{x}{l},\ Y=\frac{y}{L},\ U=\frac{u}{u_0},\ V=\frac{v}{v_0}, \tag{5}$$

$$l=\frac{j_0 M_0 a^4}{8\pi^3\rho\upsilon^2},\ L=\frac{a}{\pi},\ u_0=\frac{\pi^2\upsilon l}{a^2}=\frac{j_0 M_0 a^2}{8\pi\rho\upsilon},\ v_0=\frac{\pi\upsilon}{a}=\frac{\upsilon}{L}, \tag{6}$$

we observe that the balance equations (2), (3) and the boundary conditions (4) go over in the non-dimensional forms

$$\frac{\partial U}{\partial X}+\frac{\partial V}{\partial Y}=0, \tag{7}$$

$$U\frac{\partial U}{\partial X}+V\frac{\partial U}{\partial Y}=\frac{\partial^2 U}{\partial Y^2}+\mathrm{e}^{-Y}, \tag{8}$$

$$U|_{Y=0}=0,\quad V|_{Y=0}=-V_0,\quad U|_{Y\to\infty}\to 0. \tag{9}$$

A very basic feature of this GLG boundary-layer flow is that its dimensionless governing equations (7)–(9) are independent of the fluid properties ρ and υ, the magnetic properties j_0 and M_0, as well as the structural property a of the plate. In other words, the EMHD free-convection boundary-layer flow driven over a Riga-plate by the wall-parallel Lorentz force possesses *universal* characteristics.

3 Characteristics of the velocity field

Equations (7–9) specify a two-dimensional parabolic problem. Such a flow has a dominant velocity component U in the direction along the plate. We have solved these equations directly by using the finite-difference method of Patankar [24]. The solution procedure starts with a trial velocity distribution at the plate edge ($X=0$) and marches along the plate. At the plate edge the trial velocity was taken uniform with a very small value. At each downstream position the discretized equation (8) is solved using the tridiagonal matrix algorithm (TDMA). Subsequently the cross-stream velocity component V was obtained from the continuity equation. The forward step size ΔX increases in proportion to the width of the calculation domain and was 1% of the outer boundary. In order to obtain a complete form of the velocity profile, we used a nonuniform lateral grid. ΔY takes small values near the surface (many grid points near the surface) and increases along Y. The number of lateral grid cells was 500. The boundary-layer thickness changes along X. For that reason, the calculation domain must always be at least equal or wider than the boundary-layer thickness. Here an expanding grid has been used according to the equation

$$Y_{\text{out}}=Y_0+cX, \tag{10}$$

where Y_{out} is the outer boundary of the calculation domain, c is the spreading rate of the outer boundary and X is the distance at the current step (see Fig. 2). In every case we tried to have a calculation domain wider than the real boundary-layer thickness. This was done by trial and error. If the calculation domain was thin, the velocity profiles were truncated. In this case we used another wider calculation domain to capture the entire velocity profile. This was done by changing the coefficient c in (10).

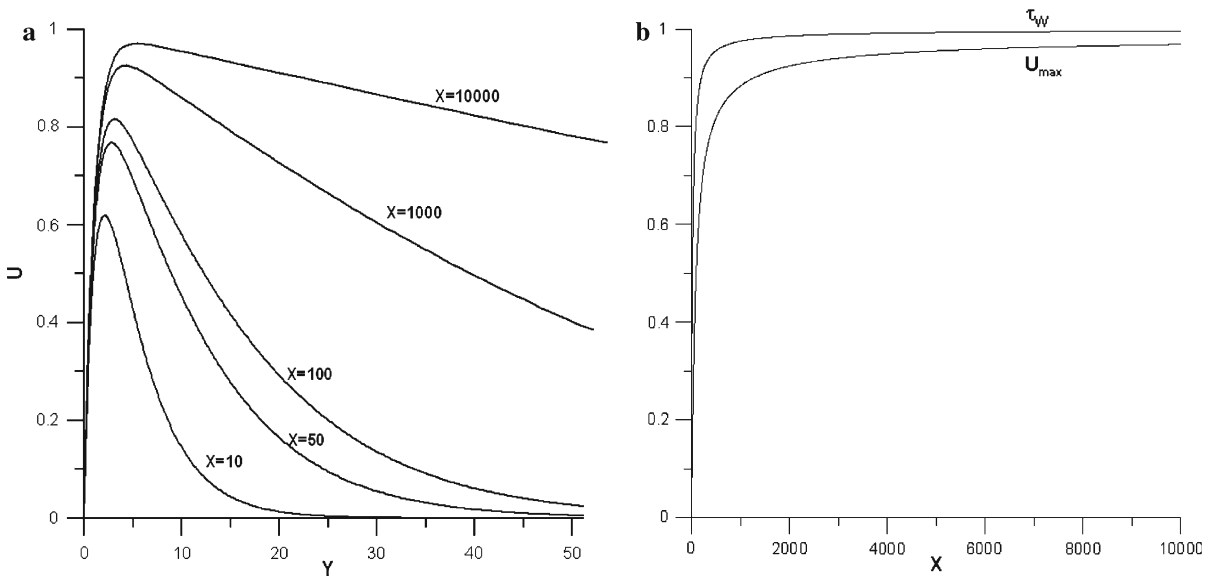

Fig. 3 **a** Mainstream velocity profiles over the impermeable plate ($V_0 = 0$) at different dimensionless distances X from the leading edge. **b** Dependence of the maximum velocity $U_{\max}(X)$ and of the skin friction $\tau_w(X)$ on X for the mainstream velocity profiles shown in Fig. 3a

Table 1 Values of the skin friction τ_w, the maximum velocity $U_{\max}$ and of its distance $Y = Y_{\max}$ from the impermeable plate ($V_0 = 0$), at different distances X from the leading edge. With increasing X, the maximum velocity and the skin friction, both approach the value 1

X	τ_w	$U_{\max}$	$Y_{\max}$ (exact)	$Y_{\max} = -\log(1-\tau_w)$ (Eq. 29)
10	0.8727	0.6135	2.1225	2.0612
20	0.9011	0.6746	2.3669	2.3136
50	0.9357	0.7604	2.8769	2.7442
100	0.9537	0.8121	3.1096	3.0726
500	0.9790	0.8974	3.8995	3.8632
1000	0.9858	0.9241	4.2943	4.2545
5000	0.9939	0.9598	5.0927	5.0994
10000	0.9967	0.9707	5.5657	5.7138

3.1 Impermeable plate

In Fig. 3a the mainstream velocity profiles $U(X, Y)$ are shown as functions of Y at different dimensionless distances X from the plate leading edge. It is seen that the thickness of the velocity boundary layer, the maximum velocity $U_{\max} = U_{\max}(X)$ and the dimensionless skin friction $\tau_w(X) = \partial U/\partial Y|_{Y=0}$ (which, from a geometrical point of view, represents the slope of the mainstream velocity profiles at the wall), all increase with increasing values of X. This X-dependence of $U_{\max}(X)$ and $\tau_w(X)$ is plotted in Fig. 3b. The asymptotic behavior seen in Fig. 3b is confirmed by the results of our numerical calculations. The maximum velocity and the skin friction, both approach the value 1 as $X \to +\infty$,

$$\lim_{X\to\infty} U_{\max}(X) = \lim_{X\to\infty} \tau_w(X) = 1. \tag{11}$$

At the same time the thickness of the boundary layer goes to infinity. A selection of the corresponding numerical values of τ_w, $U_{\max}$ and $Y_{\max}$ is collected in Table 1.

3.2 Uniform suction

We first consider the exactly solvable case which describes the *asymptotic suction profile*. The asymptotic suction profile is approached far away from the leading edge and results in the *quasi-parallel-flow* solution

$$U = U\,(Y;\, V_0)\,, \quad V = \text{const.} = -V_0 \tag{12}$$

of the problem (7–9). It is easily obtained by elementary integrations and has the form

$$U = \frac{\mathrm{e}^{-Y} - \mathrm{e}^{-V_0 Y}}{V_0 - 1}, \quad \text{for } V_0 \neq 1 \tag{13a}$$

and

$$U = Y\mathrm{e}^{-Y}, \quad \text{for } V_0 = 1, \tag{13b}$$

respectively.

The slope of all the velocity profiles (13) at the wall, i.e., the dimensionless skin friction, is the same for all values of the suction velocity V_0, namely

$$U'\,(0;\, V_0) = 1, \tag{14}$$

where a prime denotes differentiation with respect to Y. The velocity (13) reaches the maximum value

$$U_{\max}\,(V_0) = V_0^{\frac{V_0}{1-V_0}} \tag{15}$$

at

$$Y \equiv Y_{\max}\,(V_0) = \frac{\log\,(V_0)}{V_0 - 1}. \tag{16}$$

It is easy to show that $U_{\max}$ and $Y_{\max}$ given by Eqs. 15 and 16 are related to each other by the simple relationship

$$V_0 U_{\max} \exp\,(Y_{\max}) = 1 \tag{17}$$

In the case $V_0 \to 1$, Eqs. 15 and 16 go over in $U_{\max} = 1/\mathrm{e} = 0.36788$ and $Y_{\max} = 1$, respectively, in full agreement with Eqs. 13b and 17. Furthermore,

$$U_{\max} \to 1, \quad Y_{\max} \to +\infty \text{ as } V_0 \to 0, \tag{18}$$

$$U_{\max} \to 0, \;\; Y_{\max} \to 0 \quad \text{as } V_0 \to +\infty. \tag{19}$$

In Fig. 4 some of the velocity profiles (13) are shown for different values of V_0. In Fig. 5 the numerically calculated mainstream velocity profiles $U = U\,(X, Y;\, V_0)$ are shown for the suction velocity $V_0 = 0.1$, at different dimensionless distances X from the leading edge. We see that, as X increases, these velocity profiles approach the asymptotic suction profile, as expected. For the case shown in Fig. 5 this happens approximately at the downstream station $X = 400$. This so called *Iglisch-length*, i.e., the downstream distance $X = X_{\text{Iglisch}}\,(V_0)$ at which the boundary layer reaches its asymptotic shape, decreases as the suction velocity increases, again in full agreement with our physical expectation. The dimensionless skin friction $\tau_w\,(X;\, V_0) = \partial U/\partial Y|_{Y=0}$, i.e., the slope of the mainstream velocity profile at the wall, approaches the value 1 for all $V_0 > 0$ as the profiles approach the asymptotic state,

$$\tau_w\,(X;\, V_0) = 1 \quad \text{for } X \geq X_{\text{Iglisch}}\,(V_0) \;\text{ and all } V_0 > 0. \tag{20}$$

This numerical result is in full agreement with (14). The maximum velocity, as well as the distance Y of the maximum from the plate, also approaches the values given by Eqs. 15 and 16, respectively. All these features are illustrated by the numerical values collected in Table 2. In Fig. 6 the Iglisch length is plotted as a function of the suction velocity $V_0 > 0$. This characteristic (dimensionless) length is defined in practice as the distance $X = X_{\text{Iglisch}}\,(V_0)$ where $\tau_w\,(X;\, V_0)$ reaches 99% of its asymptotic value 1.

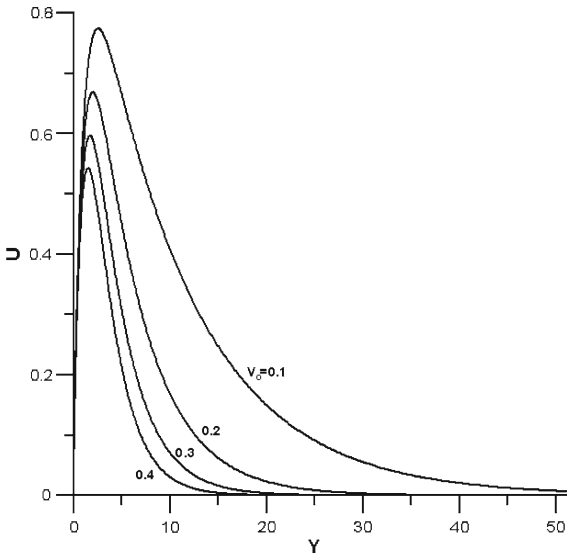

Fig. 4 Plots of the asymptotic suction profiles (13) for four different values of the suction velocity V_0

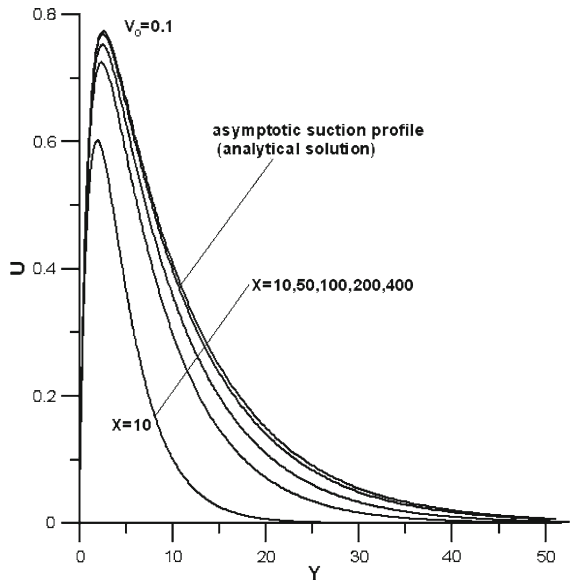

Fig. 5 Mainstream velocity profiles over the permeable plate at different dimensionless distances X from the leading edge for the suction velocity $V_0 = 0.1$

Table 2 Values of the skin friction τ_w, the maximum velocity $U_{\max}$ and of its distance $Y = Y_{\max}$ from the plate, for different suction velocities V_0 and different distances X from the leading edge. With increasing X, all these values approach the values corresponding to the asymptotic suction profile

V_0	X	Numerical solution			Asymptotic suction profile		
		τ_w	$U_{\max}$	$Y_{\max}$	τ_w	$U_{\max} = V_0^{\frac{V_0}{1-V_0}}$	$Y_{\max} = \dfrac{\log(V_0)}{V_0 - 1}$
0.1	50	0.97362	0.71801	2.32028	1	0.774264	2.55843
	100	0.98942	0.75115	2.45528			
	400	0.99980	0.77375	2.55110			
0.5	20	0.99570	0.49633	1.37516	1	0.5	1.38629
	50	0.99853	0.49908	1.37812			
	100	0.99940	0.49994	1.38235			
1	5	0.99184	0.36353	0.99532	1	0.36788	1
	10	0.99748	0.36697	0.99721			
	35	0.99901	0.36780	0.99820			
3	2	0.99428	0.19174	0.54659	1	0.19245	0.549306
	5	0.99653	0.19234	0.54814			
	7	0.99797	0.19242	0.54922			
5	1	0.99205	0.13325	0.39941	1	0.133748	0.402359
	2	0.99323	0.13344	0.40027			
	4	0.99478	0.13372	0.40178			

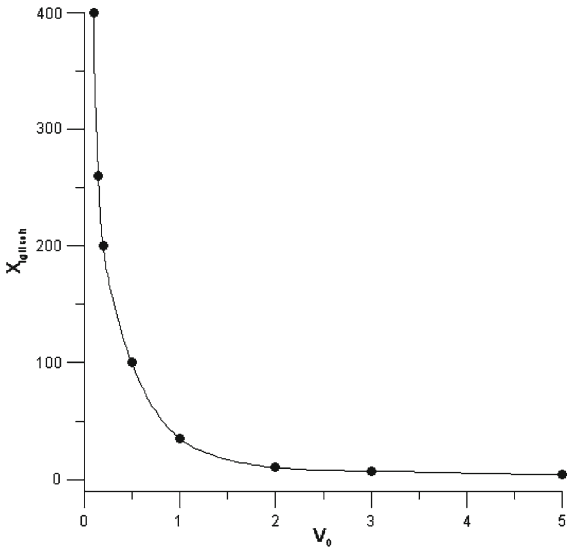

Fig. 6 The Iglish length X_{Iglisch} plotted as a function of the suction velocity V_0

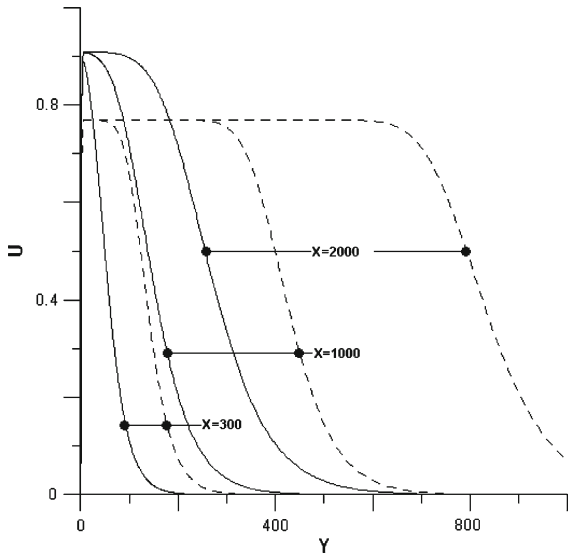

Fig. 7 Mainstream velocity profiles at different dimensionless distances X from the leading edge for the injection velocity $V_0 = -0.1$ (*solid lines*) and $V_0 = -0.3$ (*dashed lines*)

3.3 Uniform injection

In Fig. 7 some mainstream velocity profiles $U = U\,(X, Y; V_0)$ are shown for the injection velocities $V_0 = -0.1$ and $V_0 = -0.3$, and various dimensionless distances X from the leading edge. We see that, similarly to the case of uniform suction shown in Fig. 5, for a given V_0, the maximum velocity $U_{\max}\,(X; V_0)$ increases with increasing X also in this case. However, at some downstream station $X = X_*\,(V_0)$, it reaches a certain value $U_{\max}\,(X_*; V_0) \equiv U^*_{\max}\,(V_0)$ which does not change any longer when X increases further. For $V_0 = -0.1$ and $V_0 = -0.3$, this maximum value is $U^*_{\max}\,(-0.1) = 0.91$ and $U^*_{\max}\,(-0.3) = 0.77$, respectively. Therefore, in the range $X \geq X_*$ the flow consists of a central core of uniform velocity $U^*_{\max}\,(V_0)$ which is flanked at both its inner and other edge by a thin transition layer connecting the core to the homogeneous U boundary conditions (9). A remarkable quantitative feature of the flow in the range $X \geq X_*$ is that, for a given V_0, the dimensionless skin friction $\tau_w\,(X; V_0)$ also becomes independent of the coordinate X and equals the velocity $U^*_{\max}\,(V_0)$ of the central core

$$\tau_w\,(X; V_0) = U^*_{\max}\,(V_0) \quad \text{for} \quad X \geq X_* \tag{21}$$

The central core appears as a flat maximum the height of which decreases with increasing values $|V_0|$ of the injection velocity. This feature is illustrated in Figs. 8 and 9. In Fig. 8 three mainstream velocity profiles are shown for three different injection velocities $V_0 < 0$ at the downstream station $X = 10$ and in Fig. 9 the threshold $X = X_*\,(V_0)$ of the central core is plotted as a function of $|V_0|$. All the above features are illustrated by the numerical values collected in Table 3.

3.4 Analytical estimates

Our differential boundary-value problem (7–9) can be transformed (by standard manipulations) into the integral form

$$V(X, Y) = -V_0 - \int_0^Y \frac{\partial U(X, Y')}{\partial X}\,\mathrm{d}Y' \tag{22}$$

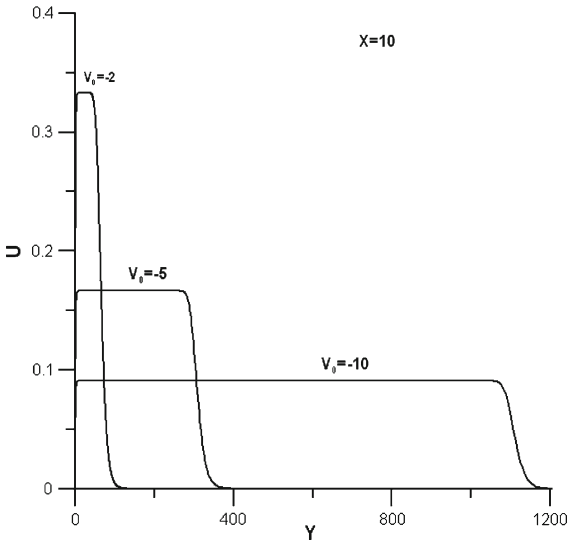

Fig. 8 Mainstream velocity profiles over the permeable plate at the dimensionless distance $X = 10$ from the leading edge for various injection velocities $V_0 < 0$

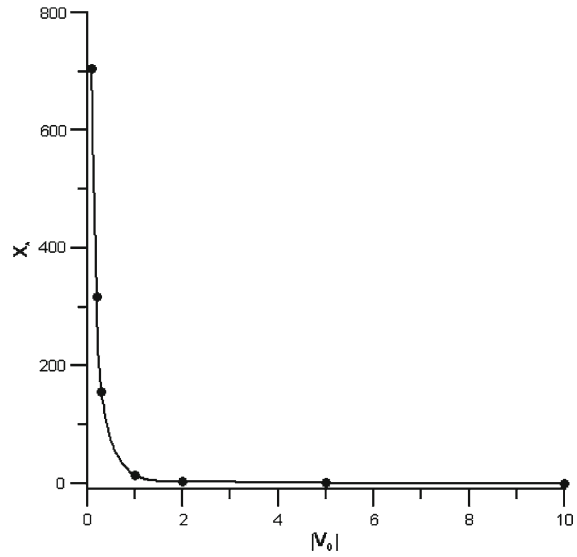

Fig. 9 Shown is, as a function of the injection velocity $V_0 < 0$, the threshold value $X_*(V_0)$ of the downstream distances X where the velocity of the central core becomes independent of X. In this range $X > X_*(V_0)$, the dimensionless skin friction $\tau_w(X; V_0)$ also becomes independent of the coordinate X and equals the velocity $U^*_{\max}(V_0)$ of the central core; see also see Table 3

$$\left[V_0 + \int_0^Y \frac{\partial U\left(X, Y'\right)}{\partial X}\,\mathrm{d}Y'\right] U(X, Y) = \mathrm{e}^{-Y} + \tau_w(X) - 1 - \frac{\partial U(X, Y)}{\partial Y} + 2\int_0^Y U\left(X, Y'\right)\frac{\partial U\left(X, Y'\right)}{\partial X}\,\mathrm{d}Y' \tag{23}$$

which is still subject to the boundary conditions

$$U|_{Y=0} = 0, \quad U|_{Y\to\infty} \to 0; \tag{24}$$

the second boundary condition (9), $V|_{Y=0} = -V_0$, is already incorporated in Eq. 22.

Letting $Y \to \infty$ in Eq. 24, we obtain for the dimensionless skin friction $\tau_w(X; V_0) = \partial U/\partial Y|_{Y=0}$ the integral formula

$$\tau_w(X) = 1 - 2\int_0^\infty U\frac{\partial U}{\partial X}\,\mathrm{d}Y \tag{25}$$

Similarly, substituting $Y = Y_{\max}(X; V_0)$ in Eq. 25, we obtain for the maximum velocity the equation

$$U_{\max}(X; V_0) = \frac{\mathrm{e}^{-Y_{\max}} + \tau_w(X) - 1 + 2\int_0^{Y_{\max}} U\frac{\partial U}{\partial X}\,\mathrm{d}Y}{V_0 + \int_0^{Y_{\max}}\frac{\partial U}{\partial X}\,\mathrm{d}Y}. \tag{26}$$

Taking into account that the two boundary conditions (24) are homogeneous, it is reasonable to define the thickness of the GLG boundary layer by the integral relationship

$$\delta(X; V_0) = \frac{\int_0^\infty U(X, Y)\,\mathrm{d}Y}{U_{\max}(X; V_0)}. \tag{27}$$

In case of an impermeable plate, $V_0 = 0$, Eq. 26 reduces to

$$U_{\max}\int_0^{Y_{\max}}\frac{\partial U}{\partial X}\,\mathrm{d}Y = \mathrm{e}^{-Y_{\max}} + \tau_w - 1 + 2\int_0^{Y_{\max}} U\frac{\partial U}{\partial X}\,\mathrm{d}Y, \tag{28}$$

Table 3 Values of the skin friction τ_w, the maximum velocity $U_{\max}$ and of the boundary-layer thickness δ, for different injection velocities V_0, at different distances X from the leading edge. With increasing X, τ_w and $U_{\max}$ approach for a given V_0 the same value $\tau_w(V_0) = U_{\max}(V_0)$ which decreases with increasing values of $|V_0|$ and is independent of X

V_0	X	$\tau_w(X; V_0)$	$U_{\max}(X; V_0)$	$\delta(X; V_0)$
−0.1	100	0.897	0.836	26.70
	300	0.907	0.889	58.60
	$X_* = 705$	0.909	0.909	115.55
	1000			154.34
	2000			282.56
−0.3	50	0.768	0.749	30.43
	100	0.769	0.766	53.80
	$X_* = 155.06$	0.769	0.769	78.77
	1000			435.95
	2000			845.12
−2	1	0.333	0.315	8.53
	2	0.333	0.330	15.12
	$X_* = 2.76$	0.333	0.333	20.17
	5			34.80
	10			66.83
−5	0.10	0.167	0.147	3.84
	0.30	0.167	0.165	10.19
	$X_* = 0.48$	0.167	0.167	16.15
	5			156.01
	10			309.29
−10	0.020	0.091	0.080	3.35
	0.050	0.091	0.089	6.76
	$X_* = 0.072$	0.091	0.091	9.35
	1			114.53
	5			559.32
	10			1113.72
	15			1669.29

Figure 3a suggests that in the range $0 \le Y \le Y_{\max}$ our U is a slowly varying function of X, i.e., $\partial U/\partial X$ is a small quantity in this interval. Accordingly, we may assume that, to leading order, the integrals in Eq. 28 are zero. Then $0 = \mathrm{e}^{-Y_{\max}} + \tau_w - 1$, i.e.

$$Y_{\max} = -\log(1 - \tau_w), \quad (V_0 = 0). \tag{29}$$

In the last column of Table 1, the values of $Y_{\max}$ as calculated from (29) are included. Compared to the "exact" numerical values of the neighboring column, a good agreement can be seen.

We turn now to the case of a permeable plate with uniform lateral suction of the fluid, $V_0 > 0$. In the special case $U = U(Y)$, one immediately recovers the asymptotic suction profiles described in Sect. 3.2. Indeed, Eqs. 22 and 25 yield $V(X, Y) = -V_0$ and $\tau_w(X) = 1$, respectively. Equation (23) reduces to

$$\frac{\mathrm{d}U}{\mathrm{d}Y} + V_0 U(Y) = \mathrm{e}^{-Y}, \tag{30}$$

which along with the boundary conditions (24) furnishes, for $V_o > 0$, the solution (13). Furthermore, Eq. 26 reduces to (17). For the thickness of the asymptotic suction profiles, Eqs. 27 and 17 give

$$\delta\left(V_0\right) = \frac{1}{V_0 U_{\max}} = V_0^{-\frac{1}{1-V_0}} = \mathrm{e}^{Y_{\max}} \tag{31}$$

According to (31), with increasing values of $Y_{\max}$, i.e., for decreasing values of the suction velocity V_0 , the thickness of the corresponding asymptotic suction profile (13) increases exponentially. This result is in full agreement with the plots shown in Fig. 4.

Figure 5 suggests that at downstream distances smaller than the Iglisch length, $X_{\text{Iglisch}}\left(V_0\right)$ the mainstream velocity $U = U\left(X, Y\right)$ is a slowly varying function of X. Thus, disregarding in (26) the integral terms (which contain the X-derivative of U), we obtain the approximation formula

$$U_{\max}\left(X; V_0\right) = \frac{\mathrm{e}^{-Y_{\max}(V_0)} + \tau_w\left(X\right) - 1}{V_0}, \quad \left(X < X_{\text{Iglisch}}\right). \tag{32}$$

This formula shows good agreement with the data of Table 2 in the range $X < X_{\text{Iglisch}}$. For example, with the data of the first row of Table 2, Eq. 32 gives for the maximum velocity $U_{\max}\left(X; V_0\right)$ the values $U_{\max}\left(50; 0.1\right) = 0.71866$ and $U_{\max}\left(100; 0.1\right) = 0.75259$ which represent good approximations compared to the exact numerical values 0.71801 and 0.75115, respectively. For $X \geq X_{\text{Iglisch}}\left(V_0\right)$, i.e., at and above the Iglisch length, as was already described in Sect. 3.2, all the characteristics of the free-convection GLG boundary-layer approach those of the asymptotic suction profile.

The integral equations given above furnish for the mainstream velocity simple approximation formulas, also in the case of uniform lateral injection of the fluid, $V_0 < 0$. Indeed, at distances $X \geq X_*$ where for a flat maximum Eq. 21 holds, in Eq. 23, in addition to the integral terms, also the exponential term $\mathrm{e}^{-Y_{\max}}$ can be neglected, such that

$$U_{\max} = \frac{\tau_w - 1}{-\left|V_0\right|} = \frac{1 - U_{\max}}{\left|V_0\right|}, \quad \left(X \geq X_*\right). \tag{33}$$

Therefore, we obtain for the velocity of the central core the simple relationship

$$U_{\max} = \frac{1}{1 + \left|V_0\right|}, \quad \left(X \geq X_*\right). \tag{34}$$

The values calculated from this approximation formula are in excellent agreement with the exact numerical value of Table 3 (in the range $X \geq X_*$).

In case of the massive injection, $\left|V_0\right| \gg 1$, a simple approximation formula can also be obtained for the boundary-layer thickness (27) in the range $X \geq X_*$. Indeed, letting $Y \to \infty$ in Eq. 22 and having in mind that for massive blowing the transversal velocity at infinity $V\left(X, \infty\right)$ can be disregarded compared to V_0, we obtain

$$\int_0^\infty \frac{\partial U}{\partial X} \mathrm{d}Y = \left|V_0\right|. \tag{35}$$

Thus, from Eq. 34 the X-derivative of (27) results in

$$\frac{\mathrm{d}\delta}{\mathrm{d}X} = \frac{1}{U_{\max}} \int_0^\infty \frac{\partial U}{\partial X} \mathrm{d}Y = \left(1 + \left|V_0\right|\right)\left|V_0\right|. \tag{36}$$

Consequently,

$$\delta\left(X; V_0\right) = \left(1 + \left|V_0\right|\right)\left|V_0\right| X, \ \left(X \geq X_*, \ \left|V_0\right| \gg 1\right). \tag{37}$$

In Table 4 the values of δ calculated from the approximation formula (37) for $V_0 = -10$ are compared to the exact numerical values of δ included in Table 3 for $X = 1, 5, 10$ and 15 (which all are larger than $X_* = 0.072$). As we see, the larger X, the higher the accuracy of (37). It is also worth mentioning here that the boundary-layer thickness given by (37) is slightly overestimated, but still is a suitable measure of the length of the plateau representing the flat maximum of the velocity profiles plotted in Fig. 8.

Table 4 Values of δ calculated from the approximation formula (37) for $V_0 = -10$, and the exact numerical values of δ included in Table 3 for $X = 1, 5, 10$ and 15. One sees that the larger X, the higher the accuracy of the approximation formula (37)

X	$\tau_w = U_{\max}$	δ_{exact}	$\delta_{\text{approx.}}\,(X; V_0)$, Eq. (37)	$100\,\frac{\delta_{\text{exact}} - \delta_{\text{approx.}}}{\delta_{\text{exact}}}$
1	0.091	114.53	110	3.955%
5		559.32	550	1.666%
10		1113.72	1100	1.232%
15		1669.29	1650	1.155%

4 Conclusions

The free-convection flow of a weakly conducting fluid from a special electromagnetic actuator, a horizontal *Riga-plate*, has been investigated by numerical and analytical methods. A spanwise aligned array of alternating electrodes and permanent magnets of a plate generates a surface-parallel Lorentz force which decreases exponentially in a direction normal to the plate. This electromagnetic body force is the only driving force of the flow. The main results of the paper can be summarized as follows.

1. There exists a certain length and velocity scale on which the flow possesses universal characteristics, i.e., characteristics which are independent of the material properties of the fluid, as well as of the structural and functional parameters of the actuator.
2. The qualitative shape of the mainstream velocity profiles induced by the horizontal Riga-plate resembles the shape of the more familiar natural-convection velocity profiles induced by a heated vertical plate (see e.g. Figs. 3a, 4 and 5). Bearing in mind that the driving forces of the two flows are physically quite different, this qualitative resemblance of the mainstream velocities is surprising. Nevertheless, there exists a formal mathematical explanation for this analogy, namely, the exponential decay with the transversal coordinate y of both the Lorentz force (see the Greenberg-term (1)) in the present case, as well as of the classical Boussinesq term in the case of natural-convection flow (see e.g. [25, Fig. 4–50, p. 326]).
3. At large downstream distances X from the leading edge of the impermeable plate, the maximum velocity $U_{\max}\,(X)$ and the dimensionless skin friction $\tau_w\,(X)$ both approach the value 1; see Fig. 3a, b.
4. The analytically available *asymptotic suction profiles* illustrate several of the qualitative features of the mainstream velocity field; see Figs. 4 and 5. The *Iglisch-length,* i.e., the downstream distance $X = X_{\text{Iglisch}}\,(V_0)$ at which the boundary layer reaches its asymptotic shape, decreases as the suction velocity increases; see Fig. 6.
5. Similar to the case of uniform suction, in the presence of uniform lateral injection of the fluid, the maximum velocity $U_{\max}\,(X; V_0)$ increases with increasing X, too. However, at some downstream station $X = X_*\,(V_0)$, it reaches a certain value $U^*_{\max}\,(V_0)$ which no longer changes when X increases further. Thus, in the range $X \geq X_*$, the flow consists of a central core of uniform velocity $U^*_{\max}\,(V_0)$ which is flanked at both its inner and other edge by a thin transition layer connecting the core to the boundary conditions. The central core appears as a flat maximum the height of which decreases with increasing values $|V_0|$ of the injection velocity; see Figs. 7–9.
6. For several characteristics of the mainstream velocity profiles reasonably accurate analytical approximation formulas have been reported; see Sect. 3.4.
7. No self-similar solutions of the present EMHD free-convection problem have been found.
8. It is also worth emphasizing again that the spanwise variations of the Lorentz force F are significant only for $y < a$. However, even in this range, the fluctuations rapidly diminish with increasing y, so that at $y = a$ the deviation of F from its average value $\langle F \rangle$ is only 2% [23, Fig. 2.9, p. 32]. This holds when the lengths h of the magnets in the direction of magnetisation amount to $0.6a$. When h is larger, the fluctuations become even smaller [23]. In this way, the boundary-layer approximation along with the Grinberg approximation yield physically reliable results.

References

1. Gailitis A, Lielausis O (1961) On a possibility to reduce the hydrodynamic resistance of a plate in an electrolyte. Appl Magnetohydrodyn Rep Phys Inst Riga 12:143–146
2. Avilov VV (1998) Electric and magnetic fields for the Riga plate. Technical Report, FRZ, Rossendorf
3. Tsinober AB, Shtern AG (1967) Possibility of increasing the flow stability in a boundary layer by means of crossed electric and magnetic fields. Magnetohydrodynamics 3:103–105
4. Grinberg E (1961) On determination of properties of some potential fields. Appl Magnetohydrodyn Rep Phys Inst Riga 12:147–154
5. Nosenchuck DM, Brown GL (1993) Direct spatial control of wall shear stress in a turbulent boundary layer. In: So RMC, Speziale CG, Launder BE (eds) Near wall turbulent flows. Elsevier, New York, pp 689–698
6. Meng JCS, Henoch C, Hubers JD (1994) Seawater electrohydrodynamics: a new frontier. Magnetohydrodyn 30:401–418
7. Henoch C, Stace J (1995) Experimental investigation of a salt-water turbulent boundary-layer modified by an applied streamwise magnetohydrodynamic body force. Phys Fluids 7:1371–1383. doi:10.1063/1.868525
8. Crawford CH, Karniadakis GE (1997) Reynolds stress analysis of EMHD-controlled wall turbulence. 1. Streamwise forcing. Phys Fluids 9:788–806. doi:10.1063/1.869210
9. O'Sullivan PL, Biringen S (1998) Direct numerical simulation of low Reynolds number turbulent channel flow with EMHD control. Phys Fluids 10:1169–1181. doi:10.1063/1.869641
10. Kim J (1997) Boundary layer control for drag reduction: taming turbulence. In: Gerbeth G (ed) International workshop on electromagnetic boundary layer control for saltwater flows. Forschungszentrum Rossendorf
11. Berger TW, Kim J, Lee C, Lim J (2000) Turbulent boundary layer control utilizing the Lorentz force. Phys Fluids 12:631–649. doi:10.1063/1.870270
12. Pang J, Choi KS (2004) Turbulent drag reduction by Lorentz force oscillation. Phys Fluids 16:L35–L38. doi:10.1063/1.1689711
13. Mutschke G, Gerbeth G, Albrecht T, Grundmann R (2006) Separation control at hydrofoils using Lorentz forces. Eur J Mech B Fluids 25:137–152. doi:10.1016/j.euromechflu.2005.05.002
14. Kim SJ, Lee CM (2000) Investigation of the flow around a circular cylinder under the influence of an electromagnetic force. Exp Fluids 28:252–260. doi:10.1007/s003480050385
15. Posdziechp O, Grundmann R (2001) Electromagnetic control of seawater flow around circular cylinders. Eur J Mech B Fluids 20:255–274. doi:10.1016/S0997-7546(00)01111-0
16. Breuer KS, Park J, Henoch C (2004) Actuation and control of a turbulent channel flow using Lorentz forces. Phys Fluids 16:897–907. doi:10.1063/1.1647142
17. Shatrov V, Gerbeth G (2007) Magnetohydrodynamic drag reduction and its efficiency. Phys Fluids 19(035109):1–12
18. Weier T, Gerbeth G, Mutschke G, Lielausis O, Lammers G (2003) Control of flow separation using electromagnetic forces. Flow Turbul Combus 71:5–17. doi:10.1023/B:APPL.0000014922.98309.21
19. Weier T, Gerbeth G (2004) Control of separated flows by time periodic Lorentz forces. Eur J Mech B Fluids 23:835–849. doi:10.1016/j.euromechflu.2004.04.004
20. Du YQ, Karniadakis GE (2000) Suppressing wall turbulence by means of a transverse traveling wave. Science 288:1230–1234. doi:10.1126/science.288.5469.1230
21. Du YQ, Symeonidis V, Karniadakis GE (2002) Drag reduction in wall-bounded turbulence via a transverse traveling wave. J Fluid Mech 457:1–34. doi:10.1017/S0022112001007613
22. Albrecht T, Grundmann R, Mutschke G, Gerbeth G (2006) On the stability of the boundary layer subject to a wall-parallel Lorentz force. Phys Fluids 18(098103):1–4
23. Weier T (2005) Elektromagnetische Strömungskontrolle mit wandparallelen Lorentzkräften in schwach leitfähigen Fluiden. Dissertation, Technische Universität Dresden, 252 pp
24. Patankar SV (1980) Numerical heat transfer and fluid flow. McGraw-Hill, New York
25. White FM (1991) Viscous fluid flow, 2nd edn. McGraw-Hill, New York